



Kochi Chapter

Indian Geotechnical Conference

IGC 2022

15th – 17th December, 2022, Kochi

Mainshock-Aftershock Response Analysis of Concrete Gravity Dam-Foundation-Reservoir System

K N Ashna¹, Priti Maheshwari² and M N Viladkar³

¹Research Scholar, Department of Civil Engineering, IIT Roorkee, India

²Professor, Department of Civil Engineering, IIT Roorkee, India

³Professor (retd), Department of Civil Engineering, IIT Roorkee, India

Abstract. Current practice of seismic analysis and design of concrete gravity dams considers only the mainshock of an earthquake sequence. However, actual damage caused due to earthquake indicates that strong aftershocks also have a major impact on the structure and its performance, and hence its effect cannot and should not be ignored. The present study therefore considers the two-dimensional seismic analysis of a concrete gravity dam along with massed foundation and the reservoir. The coupled system is subjected to spectrally matched mainshock-aftershock sequences, and the response thus obtained has been compared with the case when only the mainshock earthquake ground motion is considered. Response parameters considered are the crest displacement, stress at heel, crack length, dissipated energy and the contact displacements. The results suggest that aftershocks lead to an enhancement of these response parameters in a dam that has been damaged due to mainshock but has not yet been repaired. Attempt has also been made to discuss two types of damage indices which are suitable for consideration of the cumulative effect of damage due to aftershocks. The assessment of the damage index helps in deciding whether we should consider aftershocks for further analysis.

Keywords: mainshock-aftershock, damage index, gravity dam

1 Introduction

In general, seismic analysis of structures is carried out only for the mainshock earthquake, i.e. for the ground motion that has the highest magnitude. But earthquake usually consists of foreshocks and the mainshock event followed by several aftershocks. These aftershocks can be smaller in magnitude but their effect on the cumulative damage of structures is a matter of major concern. A structure damaged due to a mainshock earthquake should be retrofitted. However, the time interval between seismic sequences may be too short to carry out such maintenance. These sequential ground motions can cause further irrecoverable deformations in an already damaged structure, especially in case the maintenance works have not been carried out in the structure. It is therefore necessary to incorporate the effects of mainshock-aftershock sequences in the seismic analysis and design of dam like structures.

The earthquake safety of concrete gravity dams was studied by Alliard and Leger [1] who also took into account the impact of aftershocks. They discovered that aftershocks caused extra damage and sliding displacements. Zhang et al. [2] studied the effect of seismic sequences on gravity dam body alone without considering the dam-reservoir-foundation interaction effect. Wang et al. [3] quantified the effects of strong aftershocks on the damage demands of concrete gravity dams considering foundation and reservoir and compared these damage demands in terms of damage indices between the as-recorded seismic sequences and the repeated earthquakes. But the foundation was considered massless which can overestimate the response parameters. Wang et al. [4] evaluated the seismic performance of dam considering direction of seismic sequence, aftershock polarity, and earthquake intensity. They concluded that changing the direction of application of earthquake significantly affected the damage, maximum displacement, and residual displacement demands of the dam. Aftershock polarity did not affect the damage pattern in a significant way. The effect of seismic sequences on the performance of concrete faced rock fill dams was investigated by Pang et al. [5]. It was realised that aftershock causes more damage to the face slab as compared

TH-11-1

to what a single main shock earthquake can cause. Zhang et al. [6] studied the effect of main shock- aftershock sequences on the foundation of the dam and proposed to consider the damage of both the dam and the foundation during seismic analysis. These strong aftershocks increased the overall damage and the plastic strains in the dam-foundation system and the cumulative effect of damage was more prominent in foundation than in the dam body. Sadeghi and Moradloo [7] tried to analyse the seismic stability of Koyna (India) and Manjil (Iran) dams subjected to aftershocks. In their study, augmented Lagrangian method was employed to model the non-linear behaviour of contact. Contact between a cracked top block and the dam body was modelled using zero thickness contact element, and friction sliding and contact opening. As compared to no crack condition, maximum horizontal crest displacement of the top block increases during aftershock, and results in permanent displacement which can affect the overall safety of the dam.

Critical review of the literature suggests that very scarce work is available with reference to the response of gravity dams to mainshock-aftershock sequences and the resulting damage characteristics. In almost all of the above studies earthquake records from a different location is used to analyse gravity dam located at a different site. Using acceleration time history from a different region to analyse a structure located at a different location is not a reliable method for design and analysis. It is a critical issue to obtain realistic ground motion from the actual location where dam is situated. So, to overcome that issue, strong ground mainshock aftershock motions were taken from databases and matched with the target spectrum of location of interest. Further, most of the studies have used the concept of linear massless foundation which can overestimate the response. Considering these aspects, an attempt has been made in this work to carry out the analysis of a gravity dam under mainshock-aftershock sequences.

For this purpose, nonlinear finite element analysis of concrete gravity dam-foundation-reservoir system subjected to 10 spectrally matched mainshock-aftershock sequences, and its effect on response parameters has been discussed. A two-dimensional finite element model of Koyna dam in India has been used for the numerical study considering the massed foundation with absorbing boundary and nonlinear material properties. The effect of aftershock on displacements, dissipated energy and the resulting damage has been investigated. The cumulative effect of damage due to aftershocks has been discussed with two types of damage indices.

2 Finite Element Model

2.1 Dam-Foundation-Reservoir System

Koyna dam, located in the state of Maharashtra, India is selected for the present study. On December 11, 1967, an earthquake with a magnitude of 6.6 M_w struck the dam, causing cracks [8]. The Koyna dam along with foundation and reservoir is idealised as a two-dimensional structure and modelled using the commercially available software ABAQUS [9]. The foundation has a size of 351 m x 140.4 m. The reservoir has a length of 140.4 m and a depth of 91.75m. The dam, foundation and the reservoir are modelled using 8 noded quadratic rectangular elements. Foundation and dam body is modelled using plane strain and plane stress elements respectively. The dam body is modelled as plane stress because it was found that during the actual earthquake the different monoliths of Koyna dam were found to vibrate because of the presence of unkeyed contraction joints [8]. Second order acoustic elements are used to model the water body in the reservoir. Surface based fluid-structure interaction is used for representing dam-reservoir interface (upstream face of dam) and the foundation-reservoir interface. The dam-foundation interface is tied together so that no relative displacement occurs between the two.

In order to prevent the waves reflecting back to the foundation domain, standard viscous boundary proposed by Lysmer and Kuhlemeyer, [10] is used along the boundaries of rock foundation. A non-reflecting boundary condition is also applied at the far end of the reservoir body proposed by Sandler [11]. Energy dissipation in the dam-foundation-reservoir system is accounted by providing a 5% Rayleigh damping for the whole system. The mesh configuration of the considered dam-foundation-reservoir system is presented in Fig.1.

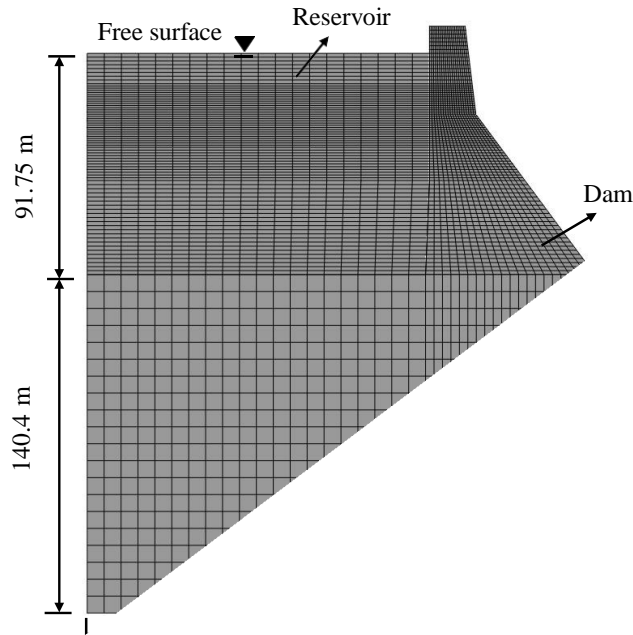


Fig. 1. Mesh configuration of the dam-foundation-reservoir system.

2.2 Constitutive Modelling and Material Properties

The concrete in the dam body is modelled using concrete damage plasticity (CDP) constitutive model proposed by Lubliner et al. [12] and Lee and Fenves [13]. Mohr-Coulomb yield criterion is used to model the rock foundation. The water in the reservoir is assumed to be inviscid, linear, and compressible. The following material properties are used in the analysis.: (a) concrete: Elastic modulus 31027 MPa, Poisson's ratio 0.2, density 2643 kg/m³, dilation angle 36.31°, initial compressive yield stress 13 MPa, ultimate compressive yield stress 24.1 MPa and Static tensile failure stress 2.9 MPa [14,9], (b) rock: Elastic Modulus 16,860, Poisson's ratio 0.18, density 2701 kg/m³, dilation angle 5° [15], (c) water: Bulk modulus 2071 MPa, density 1000 kg/m³ [16].

2.3 Application of Loads

Loads applied are as follows: self-weight of gravity dam, hydro-static pressure, uplift pressure, hydro-dynamic force and acceleration time history. Static loads are first applied followed by the dynamic loads. In this study, earthquake acceleration recorded at the ground surface is input at the top of foundation surface (dam-foundation interface) [16]. The analysis is carried out by employing Hilber-Hughes-Taylor implicit time integration method [9]. The maximum time step length chosen for each analysis is 0.005 seconds.

3 Mainshock-Aftershock Sequences

As-recorded 10 seismic sequences are taken from earthquake databases, namely, PEER [17] and COSMOS [18], and they are spectrally matched to the target design spectrum of the Koyna region where the dam is located. A time gap of 10 seconds with zero ordinate is applied between mainshock and aftershock. This gap is enough for the structure to stop moving after the mainshock event. Fig.2 displays the acceleration time history of 1980 Mammoth Lakes earthquake.

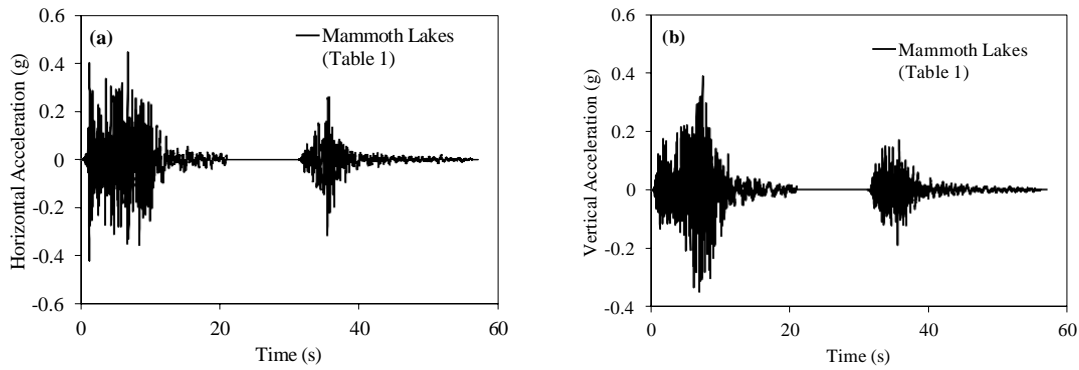


Fig. 2. As-recorded mainshock-aftershock sequence 1980 Mammoth Lakes: a) horizontal b) vertical.

The criteria followed for choosing the ground motion sequences are as follows: i) Accelerograms of mainshock and aftershock are recorded in a free-field or low height buildings to minimize the effect of soil-structure interaction, ii) Both horizontal and vertical components of ground motion are considered in this study, iii) Only single aftershock is considered with the highest magnitude. It is assumed that aftershocks of lesser magnitudes will not cause subsequent accumulated damage, iv) Magnitude of mainshock $\geq 5.0M_w$, and that of aftershocks $\geq 4.0M_w$, v) The mainshock and the corresponding aftershock occur within short period of time in which no maintenance work of dam could be carried out during the intervening period, vi) Ground motions are recorded on rock or stiff soil. Table 1 details some of the important characteristics of the selected mainshock-aftershock sequences.

3.1 Spectral Matching of Mainshock-Aftershock Sequences

Koyna dam is founded on basaltic rocks of Deccan trap. According to Indian Standard IS 1893, Part1, 2016 [19], this region falls in zone-IV of seismic zoning map of India. The design acceleration spectrum for zone- IV for structures founded on rock or hard soils and corresponding to 5% damping is shown in Fig.3. The spectrum for vertical accelerogram is taken as two-third of the horizontal [19]. The selected as-recorded seismic sequences are spectrally matched with the design spectrum obtained using SeismoMatch software by SeismoSoft[20] which is based on the wavelet algorithm proposed by Abrahamson [21] and Hancock et al. [22]. Attempt has been made to check that both mainshock and aftershock match with the design target spectrum.

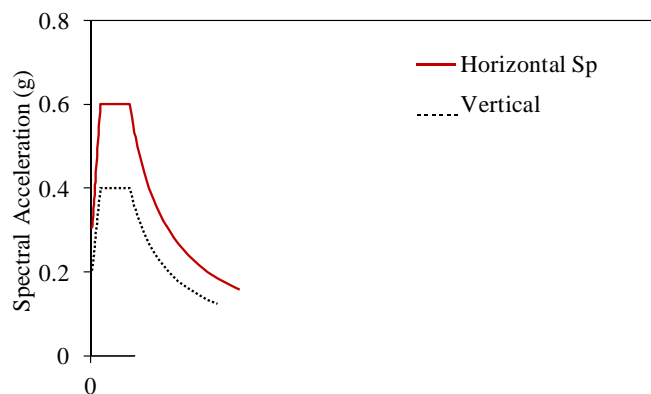


Fig.3. Target response spectra according to IS 1893, Part-1 (2016) for 5% damping

Table 1. Selected Mainshock-Aftershock sequences

Record No.	Ground Motion (Station)	Date	Event	Magnitude	Component	PGA(g)	Epicentral distance (km)	Source
1	Northridge, USA (Castaic old bridge route)	17/1/1994	Mainshock	6.69 M_w	90° (E-W) Vertical	0.568 0.217	20.72	DEFD
		17/1/1994	Aftershock	5.93 M_w	90° (E-W) Vertical	0.138 0.061	25.17	
2	Mammoth Lakes, USA (Convict creek)	27/5/1980	Mainshock	6.06 M_w	180° (N-S) Vertical	0.440 0.189	6.63	DEFD
		27/5/1980	Aftershock	5.94 M_w	180° (N-S) Vertical	0.314 0.082	12.30	
3	Whittier Narrows, USA (24461)	1/10/1987	Mainshock	6.1 M_L	270° (E-W) Vertical	0.382 0.177	0.00	COSMOS
		4/10/1987	Aftershock	5.3 M_L	270° (E-W) Vertical	0.214 0.174	14.00	
4	Cape Mendocino, USA (Petrolia)	25/04/1992	Mainshock	6.5 M_L	270° (E-W) Vertical	0.334 0.078	20.00	COSMOS
		26/04/1992	Aftershock	6.3 M_L	270° (E-W) Vertical	0.395 0.059	12.00	
5	Irpinia, Italy (Calitri)	23/11/1980	Mainshock	6.9 M_w	270° (E-W) Vertical	0.136 0.169	17.64	DEFD
		23/11/1980	Aftershock	6.2 M_w	270° (E-W) Vertical	0.176 0.158	22.22	
6	Friuli, Italy (San Rocco)	15/9/1976	Mainshock	5.91 M_w	0° (N-S) Vertical	0.134 0.058	14.50	DEFD
		11/9/1976	Aftershock	5.5 M_w	0° (N-S) Vertical	0.090 0.045	16.21	
7	Bhuj, India (Ahmedabad)	26/01/2011	Mainshock	7.0 M_b	N 78° E Vertical	0.100 0.007	239.00	COSMOS
		03/02/2011	Aftershock	5.3 M_b	N 77° E Vertical	0.023 0.015	05.00	
8	Livermore, USA (Eastman Kodak)	24/01/1980	Mainshock	5.8 M_w	180° (N-S) Vertical	0.149 0.037	17.24	DEFD
		27/01/1980	Aftershock	5.42 M_w	180° (N-S) Vertical	0.279 0.042	12.22	
9	Chi-Chi, Taiwan (CHY074)	20/09/1999	Mainshock	7.62 M_w	E Vertical	0.234 0.099	10.20	DEFD
		20/09/1999	Aftershock	6.2 M_w	E Vertical	0.062 0.029	22.60	
10	Chalfant Valley, USA (Zack brothers ranch)	21/07/86	Mainshock	6.4 M_L	360° (N-S) Vertical	0.402 0.270	12.00	COSMOS
		21/07/86	Aftershock	5.6 M_L	360° (N-S) Vertical	0.103 0.077	10.00	

4 Results and Discussions

4.1 Maximum Crest Displacement and Residual Displacements

The time histories of crest displacements of 1980 Mammoth Lakes earthquake are presented in Fig. 4. Further, the peak horizontal crest displacement obtained for single mainshock and seismic sequences are presented in Fig. 5 for all the ten earthquake sequences of Table 1. It can be observed that: i) Peak horizontal displacements

increased when the dam was subjected to aftershock sequence motions whereas the peak vertical displacement increased depending upon the ground motion, ii) On an average, seismic sequences cause more displacement demands as compared to single mainshock. and iii) Dam exhibits residual displacements which get accumulated due to earthquake and results from the finite element analysis show that seismic sequences increase the accumulated horizontal as well as vertical residual displacements. Wang et al [3], Wang et al. [4] and Sadeghi and Moradloo [7] also concluded that seismic sequences cause increased displacement responses as compared to single mainshock.

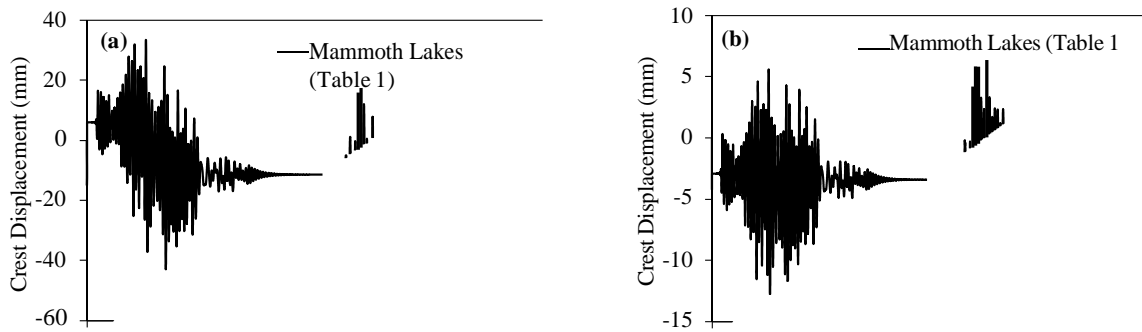


Fig.4. Crest displacement due to 1980 Mammoth Lakes sequential ground motions: a) horizontal b) vertical.

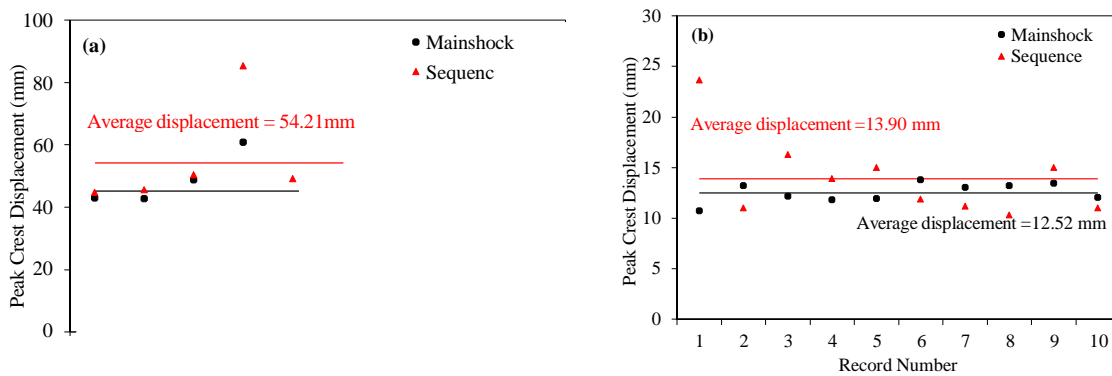


Fig.5. Peak displacement due to mainshock and after shock seismic sequences: (a) horizontal b) vertical (Refer to Table 1 for record number).

4.2 Crack Propagation

Structural damage is reflected by the propagation of cracks in the dam body. Crack length increases due to the effect of aftershocks. The propagation of cracks at the end of mainshock and mainshock-aftershock sequences is shown in Fig.6 for all the earthquakes listed in Table 1. The area where the dam body experiences tensile damage is depicted in red colour. It is clearly visible from Fig. 6 that the structure that has already undergone damage due to the main earthquake event experiences additional tensile damage due to the effect of aftershocks. Even though the magnitude of aftershocks is less than that of the mainshock, the presence of already existing cracks facilitates further extension of cracks. When the structure experiences aftershocks, either the crack propagates further from the area where it had already damaged or a new crack is initiated. The above observations are in line with findings reported in other studies [2,3,4].

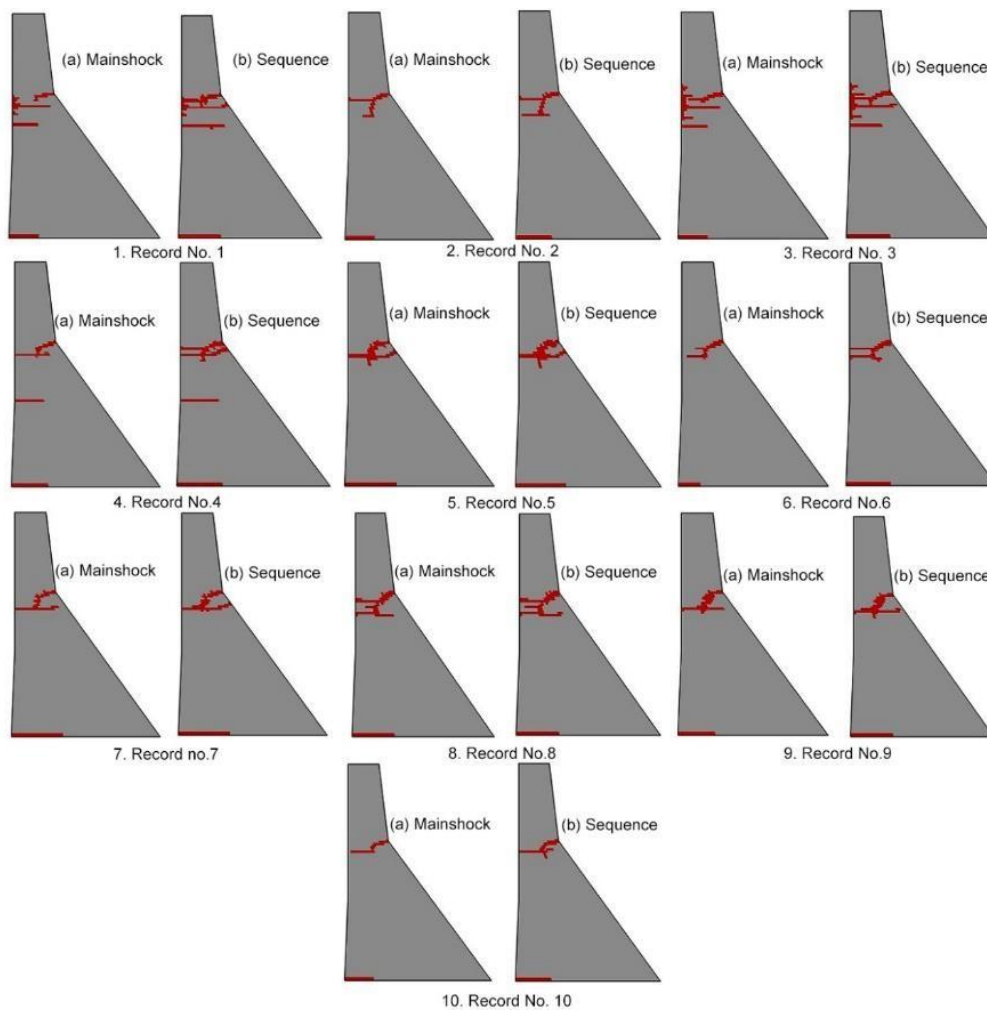


Fig.6. Crack propagation at the end of mainshock and mainshock-aftershock sequences (Table 1).

4.3 Energy Dissipated Due to Damage

Another important feature that can represent the cumulative effect of damage to the structure is the dissipated energy. It represents the energy that is released due to tensile damage happening in the dam structure. Time history of energy that is dissipated due to damage for four different seismic sequences is presented in Fig.7a. It shows that there is substantial amount of increase in the energy that is dissipated due to seismic sequences. Increased structural damage results in increased dissipated energy. Figure 7b clearly shows the difference in the amount of energy dissipated during damage due to the effect of single ground motion and ground motion sequences (Table 1). On an average there is 37.9% increase in the dissipated energy due to the effect of aftershock. Zhang et al. [6], Wang et al. [3], and Wang et al. [4] also concluded from their analyses that strong aftershocks have the potential to induce additional damage dissipated energy.

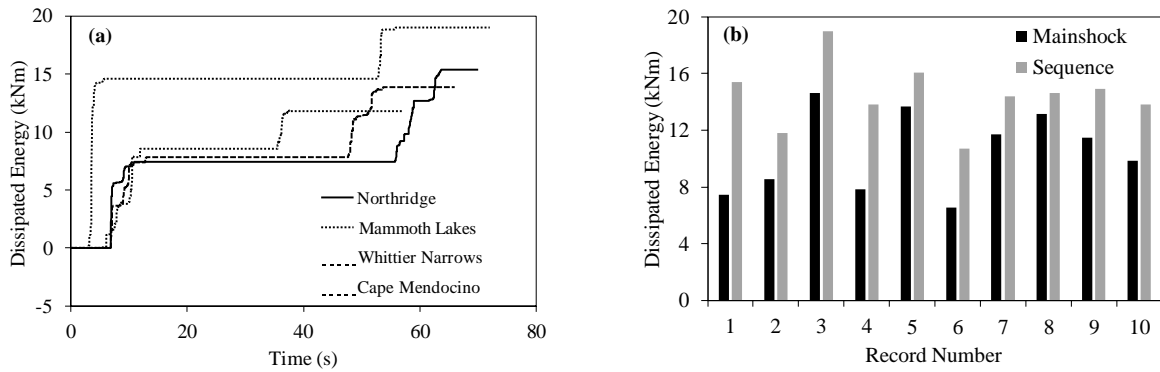


Fig.7. Variation of damage dissipated energy due to mainshock-aftershock sequences: (a) Time history of energy dissipated by damage for four different earthquake sequences (Table 1) (b) Peak value of dissipated energy for mainshock and mainshock-aftershock sequences for all records (Table 1).

4.4 Damage Index

Damage index (DI) is a normalised quantity whose value varies from 0 and 1, where 0 represents no damage condition and 1 represents the fully damaged structure. Damage index can be cumulative and non-cumulative. In the analysis of structures subjected to aftershock sequences, cumulative DIs are preferred since we are more interested in the progressive damage. Cumulative DIs proposed by Hariri-Ardebili and Saumo [23] and Ansari and Agarwal [24] have been used in this study to incorporate aftershock induced accumulated structural damage and is detailed in this section.

Damage index and damage state by Hariri-Ardebili and Saumo, 2015 [23]. Hariri-Ardebili and Saumo, 2015 [23] defined a cumulative damage index which is a function of crack length, energy dissipated, and maximum displacement at any point of interest. For each critical location in the dam body, a micro damage index, DI is defined as:

$$DI = \beta \times \frac{L_c}{L_T} \quad (1)$$

where β is the controlling coefficient, which is calculated on basis of the displacement of the point of interest, L_c is cracked length, L_T is total possible length of crack at the end of the simulation.

$$\beta = \begin{cases} \Gamma, & \text{if } \left| \frac{u_{max}}{H_{dam}} \times 100\% \right| < 0.1\% \\ 1.00, & \text{if } \left| \frac{u_{max}}{H_{dam}} \times 100\% \right| \geq 0.1\% \end{cases} \quad (2)$$

where $0.9 < \Gamma < 1$ is the reduction factor, u_{max} is maximum drift at the end of simulation which is calculated based on the location of crack, and H_{dam} is the total height of the dam.

In this study, an attempt was made to extend this damage index to concrete gravity dams subjected to mainshock-aftershock sequences. The critical locations where damage is mostly observed in a concrete gravity dam are the base and the neck of dam, where slope changes abruptly.

The micro DI and the dissipated energy due to damage is then combined to obtain a meta DI at each critical location defined as:

$$\bar{DI} = \sum_{i=1}^n DI \times \zeta \quad (3)$$

ζ is the ratio of damage dissipated energy along a crack path to the total dissipated energy in the system. Finally, macro DI for the entire dam-foundation system is defined as:

$$\bar{\bar{DI}} = \sum DI \quad (4)$$

Hence, meta damage index is calculated at two critical locations: at heel of dam and at the neck of dam body as depicted in Figs. 8a and 8b.

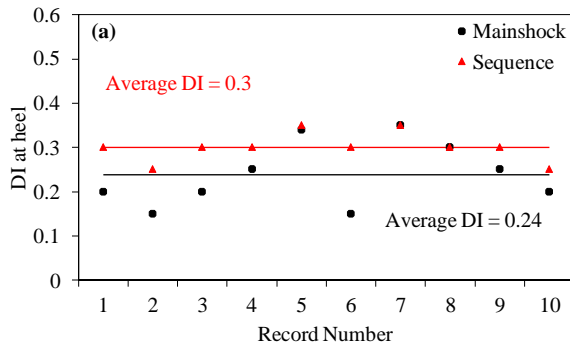


Fig. 8. Meta damage Index calculated: a) at heel of dam body (b) at neck of dam body for various mainshock-aftershock sequences (Table 1)

Accumulated crack length is reflected in this damage index. Therefore, when aftershock is applied to the dam that has already cracked previously, crack propagates further if ground motion is strong enough, thereby increasing the damage index. Overall, damage index increases when aftershock acts on the dam structure. It can be observed in Fig.9 that there is an increase of 24% in the macro-damage index due to the effect of aftershocks. The average increase in the damage index at heel of dam is 8% whereas that for the neck region is 16% indicating that neck part of the dam is more prone to structural damage due to aftershocks. Based on the damage index, several damage states were defined by Hariri-Ardebili and Saumo, 2015 [23] as follows: i) Intact, $\bar{D} = 0.00$ ii) Slight, $0.00 < \bar{D} \leq 0.10$ iii) Moderate, $0.10 < \bar{D} \leq 0.30$ iv) Severe, $0.30 < \bar{D} \leq 0.60$ v) Near Collapse, $0.60 < \bar{D} \leq 0.99$ vi) Collapse, $\bar{D} = 1.00$

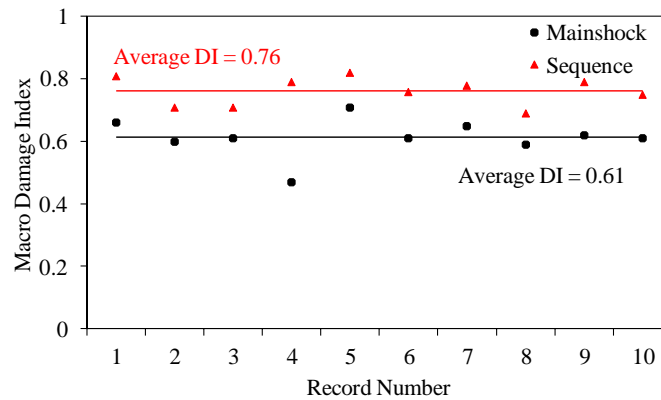


Fig. 9. Macro-damage index calculated for the whole dam for various mainshock-aftershock sequences (Table 1)

In this study, macro damage index obtained for Koyna dam corresponding to 1992 Cape Mendocino earthquake (Table 1) post mainshock ground motion was 0.47 which falls into the ‘severe’ damage state category. After the mainshock-aftershock sequence event, the value of damage index increased to 0.79. Therefore, based on the classification described, damage state of dam changes from severe to near collapse due to seismic sequence. However, the authorities had implemented dam strengthening measures post 1967 earthquake [24] by increasing the dam section and hence Koyna dam is in a safe state since then. This present study is carried out by considering the dam geometry at the time of 1967 earthquake and is intended to study the effect of strong aftershocks.

Damage Index by Ansari and Agarwal, 2016 [25]. Damage index based on the factor of safety against sliding was proposed by Ansari and Agarwal, 2016 [25] as a measure of crack length and is extended to consider the effect of aftershock sequence. This damage index is based on the residual factor of safety against sliding that occurs due to cracks forming due to earthquake event. Thus, it addresses the overall instability of the dam. The following equations are used to evaluate the factors of safety against sliding:

For the neck portion of dam,

$$FSS = \left[\frac{\tan \phi (W-U)}{F_\phi} + \frac{cA}{F_c} \right] \times \frac{1}{P} \quad (5a)$$

and for the dam – foundation interface,

$$FSS = \left[\frac{\tan \phi_{int} (W-U)}{F_\phi} + \frac{c_{a,int}A}{F_c} \right] \times \frac{1}{P} \quad (5b)$$

in which, FSS is the factor of safety against sliding; ϕ , the angle of internal friction for concrete; ϕ_{int} , the friction angle at the interface between dam and foundation; W , the weight of the dam normal to the considered sliding plane; U , the total uplift force; c , the cohesion of concrete; $c_{a,int}$, the adhesion between the dam and foundation rock along the interface; A , the area under consideration for shear; F_ϕ , the partial factor of safety in friction; F_c , the partial safety factor with respect to adhesion; and P is the total horizontal force as per IS: 6512, 1984 [26]. For the present analysis ϕ and c are taken as 45° and 2410 kPa for the concrete body and 35° and 1470 kPa for the dam foundation interface [27].

Partial damage index for any specific crack path, DI_{FSS_i} is defined as:

$$DI_{FSS_i} = \sqrt{\left(1 - \frac{FSS_i}{FSS_f}\right)} \quad (6)$$

where, FSS_i is the factor of safety against sliding at any intermediate crack length, FSS_f is the total factor of safety against sliding of undamaged dam. The corresponding global damage index is given as:

$$DI_{FSS} = \frac{[(\sum^n (DI_{FSS})_{Base/Body}) + 0.5 \times (DI_{FSS})_{Neck}]}{n+1} \quad (7)$$

DI_{FSS} is the global damage index based on factor of safety against sliding, n is the total number of crack paths excluding the crack in the neck region.

When strong ground motion acts on the structure, cracks appear. Due to the development of cracks, there is an increase in the uplift forces acting in the damaged region. With increase in damage, FSS decreases. Due to the effect of aftershock, crack length increases. This in turn increases the uplift forces, thereby decreasing the value of FSS . This is visible in Fig.10 below.

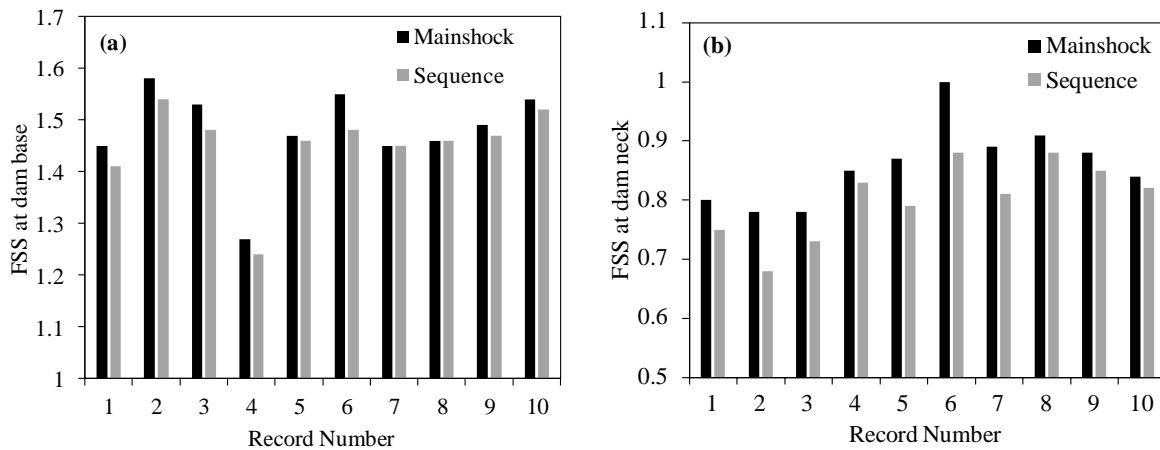


Fig. 10. Factor of safety against sliding: a) at base of dam b) at neck of dam for different main shock- aftershock sequences (Table 1)

Attempt is made here to calculate the global damage index of the Koyna dam structure at the end of mainshock and mainshock–aftershock seismic sequences, and the resulting values are plotted in Fig.11. It can be seen that the global damage index increases due to increase in the crack length.

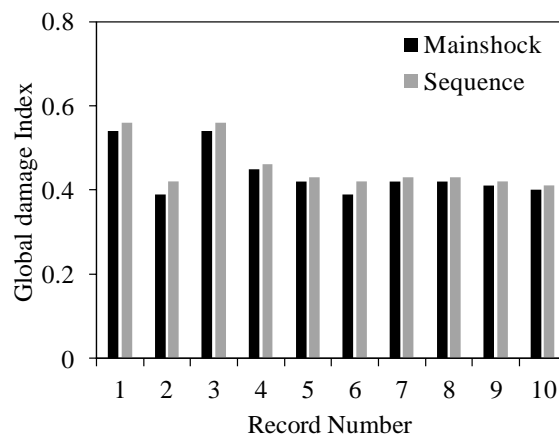


Fig. 11. Global damage index considering factor of safety against sliding (Table 1)

5 Conclusions

The response of concrete gravity dams to mainshock-aftershock sequences has been investigated in the present study. The main takeaways from the results can be summarised as follows:

- i) Mainshock-aftershock sequences result in an increased displacement demands. Peak horizontal crest displacement increases when the structure experiences aftershock ground motions. Average peak horizontal displacement increased by 20% when sequential ground motion was applied. Residual displacements also increase due to the effect of aftershocks. Increase in peak vertical displacement was also observed for certain ground motions.
- ii) Cracks propagate further from the mainshock damaged parts or new crack paths are established due to the impact of aftershock. The increased structural damage affects the integrity of the structure and inhibits the rehabilitation process after the mainshock event.
- iii) Energy dissipated due to tensile damage increases significantly when aftershock event occurs. For the earthquakes considered in this study, an average increase of 37.9% was observed. For the 1994 Northridge earthquake, energy dissipated due to tensile damage was 7.44 kNm, and for the sequential earthquake, an overall 15.39 kNm energy was dissipated.
- iv) Two types of cumulative damage indices that can be applied to concrete gravity dams subjected to mainshock ground motions have been extended to incorporate the damage caused due to mainshock-aftershock earthquake. Based on the damage index proposed by Hariri-Ardebili and Saoumo (2015), gravity dam is more prone to structural damage at neck region where the slope changes abruptly for mainshock as well as sequential ground motion. Macro damage index of dam increased from 0.61 to 0.76 i.e by 24.6% when aftershock ground motions were applied after mainshock event. Damage states of the dam are found to shift to the next damage level as a result of aftershocks. Damage index proposed by Ansari and Agarwal (2016) based on factor of safety against sliding also increases due to aftershocks. Compared to the mainshock, damage indices calculated are higher for mainshock-aftershock sequences.

The above-mentioned conclusions and observations are applicable only for Koyna concrete gravity dam when subjected to spectrally matched ten as recorded earthquake ground motions considered in this study. The other gravity dams would require detail analysis for earthquake ground motions.

References

1. Alliard, P.M., Leger, P.: Earthquake safety evaluation of gravity dams considering aftershocks and reduced drainage efficiency. *Journal of Engineering Mechanics* 134(1), 12-22 (2008).
2. Zhang, S., Wang, G., Sa, W.: Damage evaluation of concrete gravity dams under mainshock-aftershock seismic sequences. *Soil Dynamics and Earthquake Engineering* 50, 16–27 (2013).
3. Wang, G., Wang, Y., Lu, W., Yan, P., Zhou, W., Chen, M.: Damage demand assessment of mainshock-damaged concrete gravity dams subjected to aftershocks. *Soil Dynamics and Earthquake Engineering* 98, 141–154 (2017).
4. Wang, G., Wang, Y., Lu, W., Yan, P., Chen, M.: Earthquake direction effects on seismic performance of concrete gravity dams to mainshock–aftershock sequences. *Journal of Earthquake Engineering* 24(7): 1134–1155 (2018).
5. Pang, R., Xu, B., Zhang, X., Zhou, Y., Kong, X.: Seismic performance investigation of high CFRDs subjected to mainshock-aftershock sequences. *Soil Dynamics and Earthquake Engineering* 116, 82–85 (2019).
6. Zhang, L., Zhai, Y., Chen, D., Cui, X.: Study on influence of dam foundation damage on seismic safety of gravity dam under combined action of main shock and aftershock. *IOP Conference Series: Earth and Environmental Science* 304. 042063 (2019).
7. Sadeghi, M.H., Moradloo, J.: Seismic analysis of damaged concrete gravity dams subjected to mainshock-aftershock sequences. *European Journal of Environmental and Civil Engineering* 26(6),2417-2438 (2020).
8. Chopra, A.K., Chakrabarti, P.: The Koyna earthquake and the damage to Koyna dam. *Bulletin of the Seismological Society of America* 63(2), 381-397 (1973).
9. ABAQUS: Analysis user’s guide, examples problem and theory manuals (Version 6.14). Dassault Systemes Simulia Corp. Providence, RI, USA (2019).
10. Lysmer, J., Kuhlemeyer, R.L.: Finite dynamic model for infinite media. *Journal of the Engineering Mechanics* 95(4), 859–877 (1969).
11. Sandler, I.S. A new computational procedure for wave propagation problems and a new procedure for non-reflecting boundaries. *Computer Methods in Applied Mechanics and Engineering* 164, 223–233 (1998).
12. Lubliner, J., Oliver, J., Oller, S., Oñate, E.: A plastic-damage model for concrete. *International Journal of Solids and Structures* 25(3), 299–326 (1989).
13. Lee, J., Fenves, G.L.: Plastic-damage model for cyclic loading of concrete structures. *Journal of Engineering Mechanics* 124(8), 892–900 (1998).
14. Bhattacharjee, S.S., Léger, P.: Seismic cracking and energy dissipation in concrete gravity dams. *Earthquake Engineering and Structural Dynamics* 22(11), 991–1007 (1993).
15. Dhawan, K.R., Singh, D.N., Gupta, I.D.: Three-dimensional finite element analysis of underground caverns. *International Journal of Geomechanics* 4(3), 224–228 (2004).
16. Huang, J., Zerva, A.: Earthquake performance assessment of concrete gravity dams subjected to spatially varying seismic ground motions. *Structure and Infrastructure Engineering* 10(8), 1011–1026 (2014).
17. PEER, Pacific Earthquake Engineering Research Center database, <http://ngawest2.berkeley.edu/>. Last accessed: 2021/09/28.
18. COSMOS Virtual Data Center <http://strongmotioncenter.org/vdc/scripts/default.plx>. Last accessed 2021/10/25.
19. IS 1893-Part 1: Criteria for earthquake resistant design of structures, Bureau of Indian Standards, New Delhi (2016).
20. SeismoSoft: SeismoMatch- a computer program for spectrum matching of earthquake records. <http://seismosoft.com/> Last accessed 2021/07/09.
21. Abrahamson, N.A.: Non-stationary spectral matching. *Seismological Research Letters* 63(1), 30 (1992).
22. Hancock, J., Watson-Lamprey, J., Abrahamson, N.A., Bommer, J.J., Markatis, A., McCoy, E., Mendis, R.: An improved method of matching response spectra of recorded earthquake ground motion using wavelets. *Journal of Earthquake Engineering* 10(1), 67–89 (2006).
23. Hariri-Ardebili, M.A., Saouma, V.: Quantitative failure metric for gravity dams. *Earthquake Engineering and Structural Dynamics* 44(3), 461–480 (2015).
24. Paul, D.K., Chandrasekaran, A.R., Bhingare, S.L.: Identification of system parameters of the Koyna dam from accelerograms recorded on the dam. In: *Proceedings of 11th World Conference on Earthquake Engineering*, Paper No.1710, Mexico (1996).
25. Ansari, M.I., Agarwal, P.: Categorization of damage index of concrete gravity dam for the health monitoring after earthquake. *Journal of Earthquake Engineering* 20(8), 1222–1238 (2016).
26. IS 6512: Criteria for Design of Solid Gravity Dam, Bureau of Indian Standards, First Revision, New Delhi (1984).
27. Sharma, H.D. (1998), *Concrete Dams*. 2nd edn. Central Board of Irrigation and Power, New Delhi (1998).